

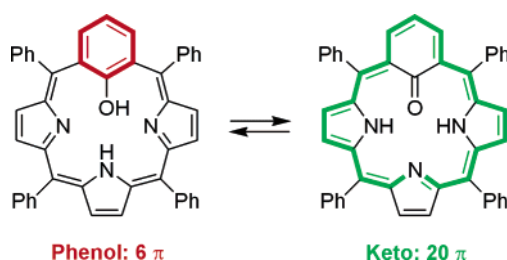
22-Hydroxybenzporphyrin: Switching of Antiaromaticity by Phenol–Keto Tautomerization

Marcin Stępień, Lechosław Latos-Grażyński,* and Ludmiła Szterenber

Wydział Chemii, Uniwersytet Wrocławski, ul. F. Joliot-Curie 14, 50-383 Wrocław, Poland

llg@wchuwr.chem.uni.wroc.pl

Received November 14, 2006



22-Hydroxybenzporphyrin, a porphyrin analogue containing a phenol moiety, has been shown to exist as an equilibrium mixture of two distinctly different tautomers. One of them actually contains the hydroxy group and shows the local [6]annulene aromaticity in the phenol fragment. The other tautomer contains a keto group and exhibits a [20]annulenoid structure characterized by macrocyclic antiaromaticity. The tautomerization process has been investigated in detail using variable-temperature ^1H NMR spectroscopy. The process is very fast, with an estimated activation energy of ca. 30 kJ/mol. Further insight into the energetics of the tautomerization is obtained from density functional (DFT) calculations. Surprisingly, the estimated energy of the antiaromatic keto species is 3–5 kcal/mol lower than the energy of the phenolic tautomer. The geometric and magnetic manifestations of aromaticity and antiaromaticity in the two tautomers are probed using a number of computational devices, including Wiberg bond indices, resonance weights derived from the harmonic oscillator model, and nucleus-independent chemical shifts. It is shown that mixing of phenolic and keto contributions in both tautomers is stronger than that in related tautomers of phenol. This effect is caused by extensive conjugation with the tripyrrolic unit of 22-hydroxybenzporphyrin and, to a lesser extent, by intramolecular hydrogen bonding.

Introduction

One of the ways to study the phenomenon of aromaticity^{1–4} is through the synthesis of new molecules, which are often specifically designed to test various aspects of the theory or to pose new problems. This approach has led to the synthesis of structurally unusual π -electron systems that are distinguished

by the ring size,⁵ extent of fusion,⁶ curvature,^{7,8} or abnormal strain.^{9–12} The chemistry of porphyrins and their analogues

(1) Minkin, V. I.; Glukhovtsev, M. N.; Simkin, B. Ya. *Aromaticity and Antiaromaticity. Electronic and Structural Aspects*; Wiley-Interscience: New York, 1994.

(2) Garratt, P. J. *Aromaticity*; Wiley: New York, 1986.

(3) *Aromaticity, Pseudoaromaticity, Antiaromaticity. Proc. Int. Symposium held in Jerusalem 31 March 1970*; Bergmann, E. D., Pullman, B., Eds.; Israel Academy of Sciences and Humanities: Jerusalem, 1971.

(4) Schleyer, P. v. R.; Jiao, H. *Pure Appl. Chem.* **1996**, *68*, 209.

(5) Sondheimer, F. *Acc. Chem. Res.* **1972**, *5*, 81.

(6) Watson, M. D.; Fechtenkötter, A.; Müllen, K. *Chem. Rev.* **2001**, *101*, 1267.

(7) Bühl, M.; Hirsch, A. *Chem. Rev.* **2001**, *101*, 1153.

(8) Scott, L. T.; Bronstein, H. E.; Preda, D. V.; Ansems, R. B. M.; Bratcher, M. S.; Hagen, S. *Pure Appl. Chem.* **1999**, *71*, 209.

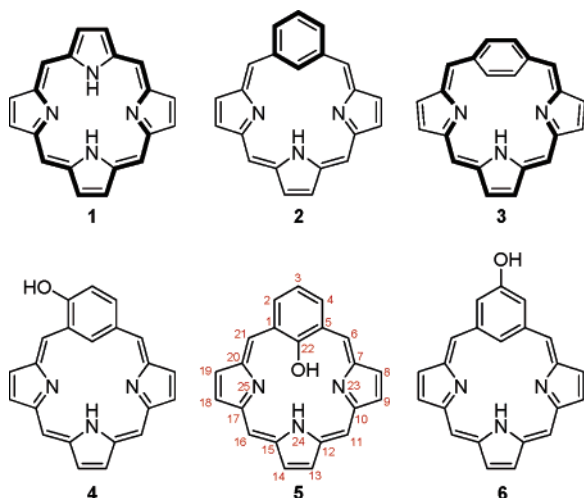
(9) Cram, D. J.; Cram, J. M. *Acc. Chem. Res.* **1971**, *4*, 204.

(10) Bodwell, G. J.; Bridson, J. N.; Cyrański, M. K.; Kennedy, J. W. J.; Krygowski, T. M.; Mannion, M. R.; Miller, D. O. *J. Org. Chem.* **2003**, *68*, 2089.

(11) Diercks, R.; Vollhardt, K. P. C. *Angew. Chem., Int. Ed. Engl.* **1986**, *25*, 266.

(12) Bürgi, H.-B.; Baldrige, K. K.; Hardcastle, K.; Frank, N. L.; Gantzel, P.; Siegel, J. S.; Ziller, J. *Angew. Chem., Int. Ed. Engl.* **1995**, *34*, 1454.

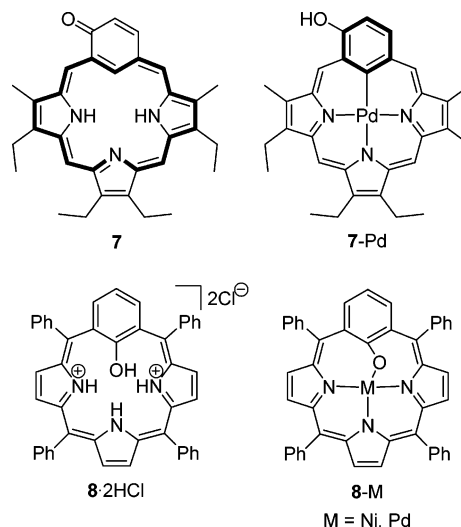
SCHEME 1



(porphyrinoids) is a particularly attractive area for such explorations, as it is centered on a structural motif (**1**, Scheme 1) that has been well studied due to its biological relevance and can be creatively altered in many ways. The aromaticity of porphyrinoids is dependent on many factors including distortion from planarity,¹³ redox chemistry,^{14,15} and tautomeric equilibria.¹⁶ It can be influenced by a variety of structural modifications, such as peripheral substitution,¹³ covalent linking of multiple macrocycles,¹⁷ ring expansion,¹⁸ and introduction of nonpyrrolic subunits.^{19,20}

The latter approach is most readily realized by replacing one of the pyrrole rings of the porphyrin with a different hetero- or carbocyclic fragment.^{19,20} Such a modification can have a profound influence on the aromaticity of the macrocycle, as demonstrated by the family of benziporphyrins,²¹ porphyrin analogues with a benzene ring substituting one of the pyrroles. Spectral characteristics and reactivity of *meta*-benzporphyrin (**2**)^{22,23} indicate that it lacks the aromatic stabilization of regular porphyrins. The macrocyclic aromaticity in **2** is disrupted by incorporation of the *meta*-phenylene ring, which is not conjugated with the tripyrrolic brace. On the other hand, *para*-benzporphyrin (**3**)²⁴ is aromatic and exhibits a strong diatropic ring current, despite the nonplanarity of the macrocycle. The aromaticity of **3** was explained in terms of a quinoidal resonance contribution, which is not available to **2**. Both compounds

SCHEME 2



perform well as ligands, and a number of their complexes were characterized, some of which stabilize metal carbon bonds²³ or weak metal–arene interactions.^{24,25}

Hydroxybenzporphyrins **4–6** (Scheme 1) are potentially interesting derivatives of benziporphyrin **2**, because their aromaticity can be controlled by tautomeric equilibria. Additionally, the hydroxy group can affect the coordinating properties of the macrocycle, acting as an additional donor or influencing the electronics of the benzene ring. A β -substituted derivative of **4** was synthesized and was shown to exist solely as the semiquinone tautomer **7** (oxybenzporphyrin, Scheme 2), in which the macrocyclic aromaticity is restored.²⁶ It was shown later that a phenolic species **7-Pd**, which is a derivative of **4**, was stabilized upon coordination of palladium(II) in the macrocyclic cavity, showing the subtle interplay between tautomerism and coordination.²⁷ While the tautomeric behavior of **4** was well established, the isomeric systems **5** and **6** remained to be explored. Recently, we succeeded in preparing metal complexes of a *meso*-substituted 22-hydroxybenzporphyrin (**8-M**).²⁸ However, 22-hydroxybenzporphyrin itself was only characterized as its diacid salt **8·2HCl**. We now report the isolation of **8** and show that it undergoes a phenol–keto tautomerization, which acts as a unique switch of antiaromaticity. The unusual antiaromatic keto form is identified at low temperatures using ¹H NMR spectroscopy. Energetics of the tautomerization and the aromaticity of the species involved are further investigated using methods of computational chemistry.

Results and Discussion

Synthesis. An apparently straightforward route to 22-hydroxybenzporphyrin was opened with the serendipitous discovery of an oxidative substitution reaction of tetraphenyl-*meta*-benzporphyrin (**9**, Scheme 3). When treated with silver(I) acetate, **9** undergoes a selective acetoxylation at the inner carbon (22-C), yielding 22-acetoxybenzporphyrin (**10**).²³ It was expected that the hydrolysis of the ester functionality in **10** would

(13) Senge, M. O. Highly Substituted Porphyrins. In *The Porphyrin Handbook*; Kadish, K. M., Smith, K. M., Guillard, R., Eds.; Academic Press: San Diego, CA, 2000; Vol. 1, Chapter 6, pp 239–347.

(14) Cosmo, R.; Kautz, C.; Meerholtz, K.; Heinze, J.; Müllen, K. *Angew. Chem., Int. Ed. Engl.* **1989**, *28*, 604.

(15) Sprutta, N.; Latos-Grażyński, L. *Chem.-Eur. J.* **2001**, *7*, 5099.

(16) Furuta, H.; Ishizuka, T.; Osuka, A.; Dejjima, H.; Nakagawa, H.; Ishikawa, Y. *J. Am. Chem. Soc.* **2001**, *123*, 6207.

(17) Aratani, N.; Osuka, A. *Chem. Rec.* **2003**, *3*, 225.

(18) Sessler, J. L.; Seidel, D. *Angew. Chem., Int. Ed.* **2003**, *42*, 5134.

(19) Latos-Grażyński, L. Core Modified Heteroanalogues of Porphyrins and Metalloporphyrins. In *The Porphyrin Handbook*; Kadish, K. M., Smith, K. M., Guillard, R., Eds.; Academic Press: New York, 2000; Vol. 2, Chapter 14, pp 361–416.

(20) Lash, T. D. Syntheses of Novel Porphyrinoid Chromophores. In *The Porphyrin Handbook*; Kadish, K. M., Smith, K. M., Guillard, R., Eds.; Academic Press: San Diego, CA, 2000; Vol. 2, Chapter 10, pp 125–199.

(21) Stępień, M.; Latos-Grażyński, L. *Acc. Chem. Res.* **2005**, *38*, 88.

(22) Berlin, K.; Breitmaier, E. *Angew. Chem., Int. Ed. Engl.* **1994**, *33*, 1246.

(23) Stępień, M.; Latos-Grażyński, L. *Chem.-Eur. J.* **2001**, *7*, 5113.

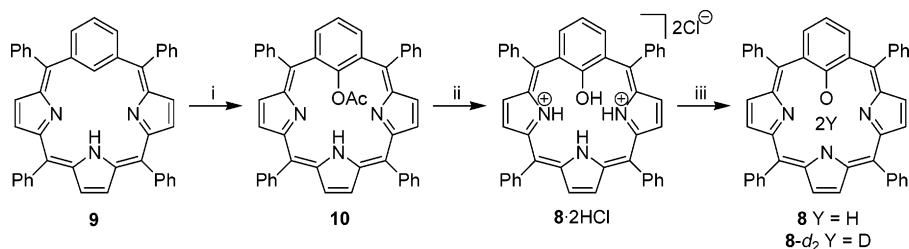
(24) Stępień, M.; Latos-Grażyński, L. *J. Am. Chem. Soc.* **2002**, *124*, 3838.

(25) Stępień, M.; Latos-Grażyński, L.; Szterenber, L.; Panek, J.; Latajka, Z. *J. Am. Chem. Soc.* **2004**, *126*, 4566.

(26) Lash, T. D. *Angew. Chem., Int. Ed. Engl.* **1995**, *34*, 2533.

(27) Stępień, M.; Latos-Grażyński, L.; Lash, T. D.; Szterenber, L. *Inorg. Chem.* **2001**, *40*, 6892.

(28) Stępień, M.; Latos-Grażyński, L. *Inorg. Chem.* **2003**, *42*, 6183.

SCHEME 3. Synthesis of 22-Hydroxybenzporphyrin **8**^a

^a Reagents and conditions: (i) CH_3COOAg , CHCl_3 , MeCN , reflux; (ii) $\text{HCl}/\text{H}_2\text{O}$, CHCl_3 , reflux; (iii) $\text{NaOH}/\text{H}_2\text{O}$ (**8**) or $\text{NaOD}/\text{D}_2\text{O}$ (**8-d₂**), CH_2Cl_2 , rt, N_2 atmosphere. **8** refers to a mixture of tautomers, without specifying the protonation pattern.

directly yield the desired 22-hydroxybenzporphyrin (**8**). Hydrolysis experiments were initially performed under a variety of basic and acidic conditions, followed by neutralization of the reaction mixture. In each case, **8** eluded identification, even though the starting material was consumed. However, when **10** was reacted with metal salts, such as NiCl_2 or PdCl_2 , the acetoxy group was cleaved to produce well-defined metal complexes with a $\text{M}-\text{O}$ bond (**8-M**, $\text{M} = \text{Ni}^{\text{II}}$, Pd^{II}).²⁸ Finally, it was discovered that when **10** was hydrolyzed with aqueous HCl in a biphasic system and no base was added during workup, **8** could be isolated in the form of its dichloride acid salt **8**·2HCl.²⁸ This salt was relatively air stable and could be thoroughly characterized.

Free **8** can be obtained by reacting solutions of the diacid with a variety of bases. However, in the presence of air and moisture, free base **8** undergoes quick decomposition (probably to *meso*-hydroxylated products²¹). Consequently, all attempts to obtain X-ray quality crystals of **8** were unsuccessful. An optimized procedure for the preparation of **8** involves stirring a dichloromethane solution of **8**·2HCl with aqueous NaOH , followed by quick separation of the organic phase and solvent removal. All of these operations are performed in an inert atmosphere to reduce the extent of decomposition.

Spectroscopic Characterization of 22-Hydroxybenzporphyrin. Alternatively, free base **8** could be obtained by titrating a solution of **8**·2HCl with diisopropylamine. The progress of such a titration was followed with UV–vis spectroscopy, as shown in Figure 1. The electronic spectrum of **8**·2HCl, reported previously,²⁸ is typical of diprotonated *m*-benzporphyrins,²³ indicating that in the dication of **8**, the electronic structure is not significantly affected by the presence of the 22-hydroxy group. Addition of ca. 2 equiv of diisopropylamine converts the orange-brown **8**·2HCl into an olive species with an electronic spectrum that is markedly different from the spectra exhibited by free base benzporphyrins (**9** and **10**).²³ In particular, an additional shoulder is present in the Soret region at ca. 460 nm, accompanied by two smaller bands in the 550–650 nm region, all of which are absent in the spectrum of **9**.²³ On the basis of the ¹H NMR evidence presented below, the olive species was identified as the free base **8**.

The intermediate stages of titration showed poorly defined isobestic points (Figure 1), indicating that the deprotonation is likely a stepwise process involving a monocationic form. On the other hand, addition of a larger excess of diisopropylamine does not produce any further changes in the UV–vis spectrum, showing that under these conditions further deprotonation is not possible. The bulkiness of diisopropylamine helps to avoid a nucleophilic attack at the *meso* positions of **8**, which is a known type of reactivity for benzporphyrins.^{21,23}

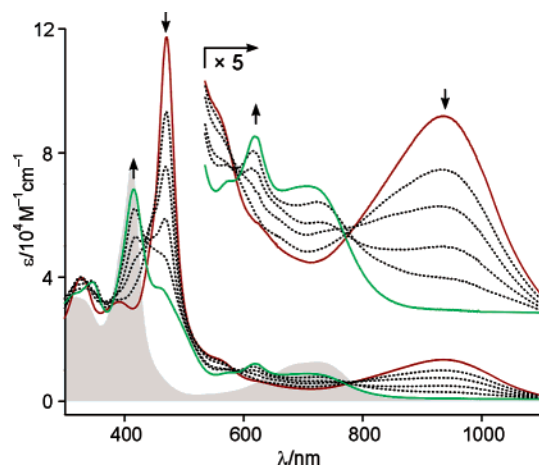


FIGURE 1. Electronic spectra (298 K, CH_2Cl_2) of the 22-hydroxybenzporphyrin dication **8**·2HCl (red line) and free base **8** (green line) obtained during a titration with diisopropylamine. Intermediate titration steps are shown as dotted lines. The reference spectrum of **9**²³ is shown as a gray silhouette.

¹H NMR Spectroscopy of 22-Hydroxybenzporphyrin. ¹H NMR spectra of **8**·2HCl were reported previously and contained no abnormal features. They were similar to the spectra obtained for the protonated *meta*-benzporphyrin, reflecting the similarity of their electronic structure. On the other hand, the ¹H NMR spectrum of the free base **8** recorded at 303 K has a fairly unusual appearance (Figure 2). The peaks are significantly broadened, which precludes recognition of splitting patterns and makes the assignment of signals difficult. Additionally, the observed chemical shifts are very different from those exhibited by other benzporphyrin derivatives. Partial assignment was achieved with the aid of a TOCSY spectrum recorded at 323 K (Figure 2). Peaks located at 6.34, 6.11, and 5.77 ppm were identified as corresponding to pyrrolic β -protons, whereas those at 5.96 and 5.53 ppm were recognized as belonging to the *m*-phenylene (3-H and 2,4-H, respectively). The latter assignment relies on the 1:2 intensity ratio of the two signals.

The line broadening observed for **8** is dynamic in character and shows a strong temperature dependence. However, the line widths vary over a wide temperature range, and it is quite difficult to observe well-resolved spectra in suitable solvents (such as dichloromethane-*d*₂ or toluene-*d*₈). This constraint is especially severe for the fast exchange limit, which could not be reached even at 373 K (toluene-*d*₈). Fortunately, when the NH and OH protons of **8** were selectively replaced with deuterons (Scheme 3), the exchange was slowed down suf-

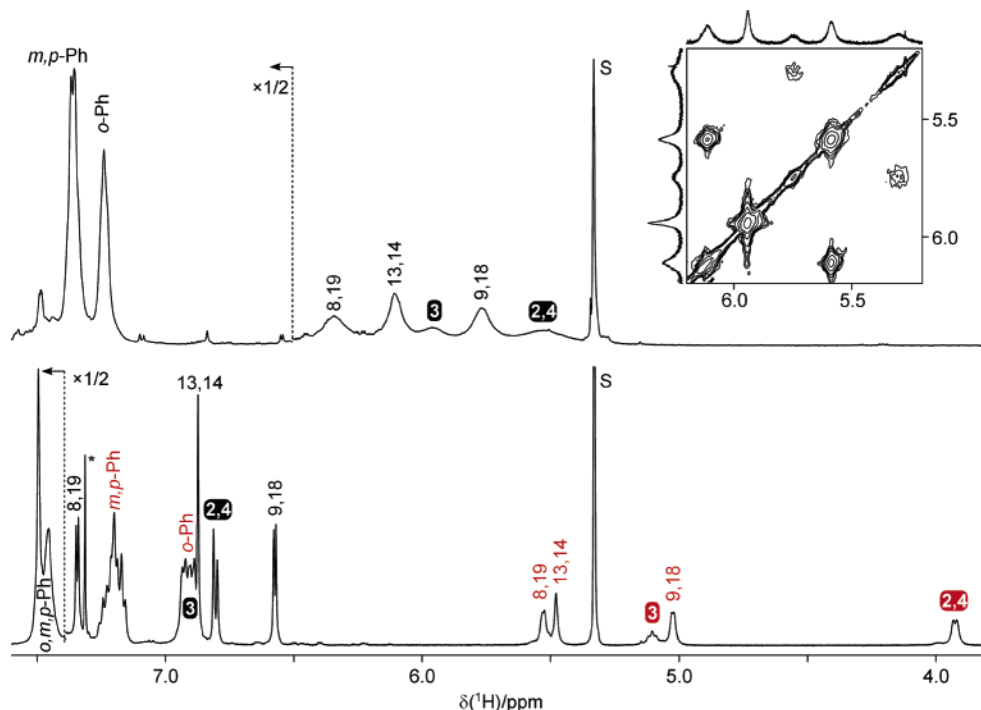


FIGURE 2. ^1H NMR spectrum of **8** (top trace, 303 K, CD_2Cl_2). The downfield region containing NH and OH signals is not shown. Peak assignments were obtained from a TOCSY spectrum (inset, 323 K, CDCl_3). ^1H NMR spectrum of $\mathbf{8-d}_2$ (bottom trace, 193 K, CD_2Cl_2). Peaks corresponding to the 22-hydroxy tautomer ($\mathbf{8}'$, Scheme 4) are labeled in black; those corresponding to the 22-oxy species ($\mathbf{8}''$) are labeled in red.

ficiently to provide reasonably narrow line widths.^{29,30} This result was also an important indication that the dynamic process is a prototropic tautomerization involving shifts of the internal protons. The deuterated derivative $\mathbf{8-d}_2$ was obtained by reacting a solution of $\mathbf{8}\cdot 2\text{HCl}$ with $\text{NaOD}/\text{D}_2\text{O}$ followed by usual workup (Scheme 3). The ^1H NMR spectrum of $\mathbf{8-d}_2$ recorded in CD_2Cl_2 at 193 K is shown in Figure 2. It consists of two sets of signals corresponding to two different tautomers of **8**. The signals were identified on the basis of two-dimensional ^1H NMR spectroscopy. In particular, the EXSY spectrum, shown in Figure 3, yielded exchange correlations between corresponding signals of the two tautomers.

The observation of the NH and OH signals, which are missing from the ^1H NMR spectrum of $\mathbf{8-d}_2$, is necessary for the interpretation of the tautomerism. Thus, a complementary set of variable-temperature spectra was recorded for a nondeuterated sample of **8** (Figure 4). Because of the larger chemical shift differences between the exchanging protons, slow exchange in this spectral region is achieved at higher temperatures than those needed for the peripheral protons. At 193 K, three signals were observed in the far-downfield region of the spectrum of **8**: two of them, at 10.34 and 8.55 ppm, had equal intensities and corresponded to one tautomer, whereas the other species was represented by a single peak at 21.0 ppm. EXSY exchange correlations between these three signals were observed even at 193 K. On raising the temperature, the signals broadened significantly and finally coalesced into a single broad peak ($\Delta\nu_{1/2} > 1$ kHz) located at 17.6 ppm (303 K).

The above spectral data can be convincingly interpreted in terms of a tautomeric equilibrium between a phenolic species, 22-hydroxybenzporphyrin $\mathbf{8}'$, which exchanges with a semi-

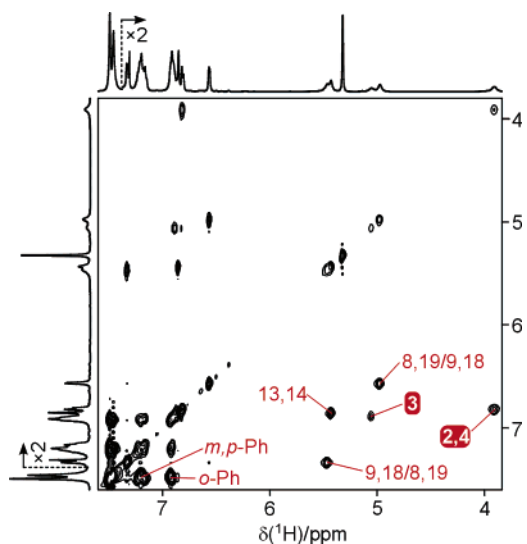


FIGURE 3. ^1H NMR EXSY spectrum of $\mathbf{8-d}_2$ (213 K, CD_2Cl_2 , $\tau_M = 0.4$ s). The only NOE correlation observed under these conditions is a cross-peak between the *o*-Ph and *m*-Ph signals of 22-oxybenzporphyrin $\mathbf{8}''$ (Scheme 4).

quinone (keto) form $\mathbf{8}''$ (Scheme 4). The latter will be termed 22-oxybenzporphyrin, in analogy to **7**. In addition, k_1 and k_{-1} will denote the overall rates of the forward ($\mathbf{8}'$ to $\mathbf{8}''$) and reverse reaction, respectively. The equilibrium constant $K = [\mathbf{8}'']/[\mathbf{8}']$ is not significantly dependent on temperature. The estimates of K obtained at 193 K (by integration) and 293 K (from averaged chemical shifts) are 0.77 and 0.84, respectively. A similar value of K was also found for the deuterated derivative (0.58 at 193 K).

The exchange between $\mathbf{8}'$ and $\mathbf{8}''$ can be regarded as an example of phenol–keto tautomerism.³¹ For simple phenols, the keto (dienone) form is not normally observed,³² but it may

(29) Abraham, R. J.; Hawkes, G. J.; Smith, K. M. *Tetrahedron Lett.* **1974**, 16, 1483.

(30) Eaton, S. S.; Eaton, G. R. *J. Am. Chem. Soc.* **1977**, 99, 1601.

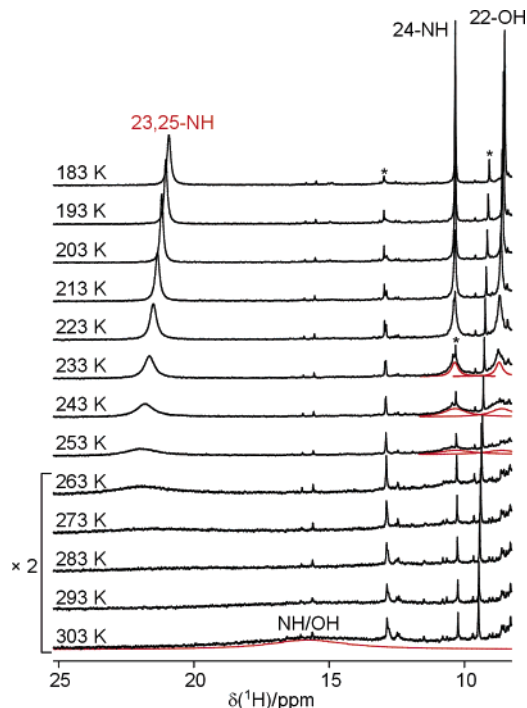
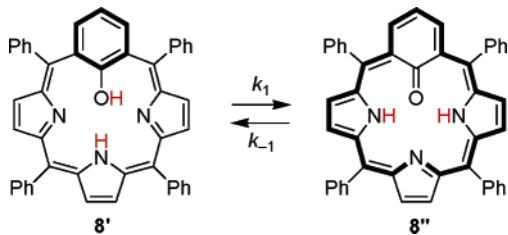


FIGURE 4. Downfield region of the ^1H NMR spectrum of **8** (183–303 K, CD_2Cl_2) containing the NH and OH signals. Red lines identify broad peaks.

SCHEME 4. Tautomerism of 22-Hydroxybenzporphyrin



become observable in more complicated systems, especially when additional functional groups are present,³³ or when the phenol contains a heterocyclic ring³⁴ or a fused aromatic system (as in anthrone³⁵). The unique feature of the present system is that the phenol–keto tautomerization is confined inside a macrocyclic framework.

The exchange process interconverting **8'** and **8''** is a combination of the phenol–keto tautomerism and the NH tautomerism typical of regular porphyrins.³⁶ On the basis of the data available for porphyrins,^{37,38} it can be expected that the exchange between **8'** and **8''** occurs with the intermediacy of a cis-protonated form,

(31) Raczyńska, E. D.; Kosińska, W.; Osmiałowski, B.; Gawinecki, R. *Chem. Rev.* **2005**, *105*, 3561.

(32) Smith, M. B.; March, J. *March's Advanced Organic Chemistry. Reactions, Mechanisms, and Structure*, 5th ed.; Wiley-Interscience: New York, 2001.

(33) Highet, R. J.; Batterham, R. J. *J. Org. Chem.* **1964**, *29*, 475.

(34) Parchment, O. G.; Burton, N. A.; Hillier, I. H.; Vincent, M. A. *J. Chem. Soc., Perkin Trans. 2* **1993**, 861.

(35) Abraham, R. J.; Mobili, M.; Smith, R. J. *Magn. Reson. Chem.* **2003**, *41*, 26.

(36) Storm, C. B.; Teklu, Y. *J. Am. Chem. Soc.* **1972**, *94*, 1745.

(37) Braun, J.; Koecher, M.; Schlabach, M.; Wehrle, B.; Limbach, H.-H.; Vogel, E. *J. Am. Chem. Soc.* **1994**, *116*, 6593.

(38) Braun, J.; Limbach, H.-H.; Williams, P. G.; Morimoto, H.; Wemmer, D. E. *J. Am. Chem. Soc.* **1996**, *118*, 7231.

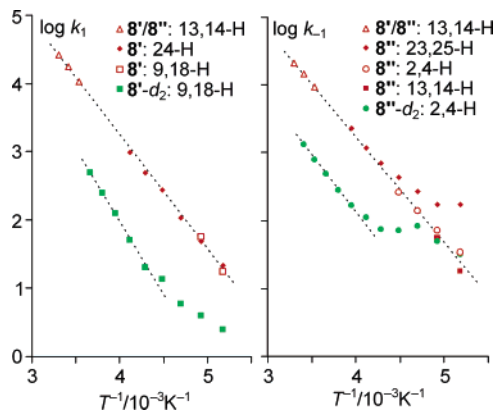


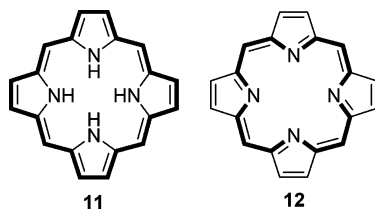
FIGURE 5. Arrhenius plots for the exchange between **8'** and **8''** (red points) and **8'-d₂** and **8''-d₂** (green points). The plots are given for the forward reaction (k_1 : **8'** to **8''**) and reverse reaction (k_{-1} : **8''** to **8'**). Dotted lines indicate regions of linearity. Data points labeled **8'/8''** correspond to the fast exchange region; those labeled **8'** or **8''** were obtained from respective slow exchange data.

and with a significant contribution of tunneling to each proton-transfer step. The observed dynamic behavior is quite complicated in terms of both the exchange pattern and the structural complexity of the involved species. Because of the lower symmetry of the macrocyclic framework of **8**, there are more nondegenerate exchange pathways than in the case of symmetrically substituted porphyrins. The incompleteness of available dynamic NMR data, which is due in part to signal overlap and in part to the limited temperature range, makes it difficult to calculate accurate activation parameters. For illustration, Arrhenius plots are given in Figure 5 that were constructed from selected line broadening data obtained for **8** and **8-d₂**. In the case of the nondeuterated species **8** (red points), the plots combine the regions of fast and slow exchange. Good linearity is obtained for k_1 over the entire range of studied temperatures, whereas for k_{-1} the temperature dependence for 23,25-H is not ideal. When the k_1 values are fitted to the Arrhenius equation, an estimate of $E_A = 32$ kJ/mol is obtained, with a frequency factor of 7.7×10^9 . This E_A value is similar to the activation energy for proton transfer in porphine determined by Limbach et al. (37 kJ/mol).³⁹ Reaction rates for **8-d₂** are slower than those for **8** (Figure 5, green points): the k_{-1}^{H} : k_{-1}^{D} ratio is approximately 11.5 at 293 K. At low temperatures, the Arrhenius plots for **8-d₂** exhibit marked nonlinearity, which is especially strong for k_{-1} , and is a consequence of additional broadening of all signals, in particular those of **8''-d₂**. A similar but weaker effect was observed for the nondeuterated sample. The line broadening observed for the keto species at low temperatures is associated with gradual changes in chemical shifts. The upfield signals of the **8''-d₂** species shift to lower field as the temperature is decreased (see the Supporting Information), whereas the 23,25-NH signal of **8''** shifts to higher field with decreasing temperature (Figure 4). On the other hand, the chemical shifts of the phenolic form **8'** remain virtually constant over the entire range of slow exchange.

One possible interpretation of this behavior assumes an additional dynamic process that affects the keto form **8''** and is much faster than the exchange between **8'** and **8''**. This additional equilibrium, possibly another prototropic tautomer-

(39) Braun, J.; Schwesinger, R.; Williams, P. G.; Morimoto, H.; Wemmer, D. E.; Limbach, H.-H. *J. Am. Chem. Soc.* **1996**, *118*, 11101.

SCHEME 5. [20]Porphyrin (Isophlorin) (11) and [16]Porphyrin (12)



ization, is temperature dependent, thus affecting the average chemical shifts observed for $8''$. Another explanation involves the presence of intramolecular low-barrier hydrogen bonds involving the inner protons of **8**. As shown by Limbach and co-workers, the presence of such bonds often results in a temperature-dependent continuum of hydrogen-bond geometries.^{40–45} This temperature dependence is induced by the properties of dichloromethane, which increases its dielectric constant at lower temperatures to favor structures with higher polarity.⁴²

Aromaticity of $8'$ and $8''$. The presence of a paratropic ring current is a commonly accepted indicator of antiaromatic character.^{46,47} Paratropicity causes shielding of the protons located on the outside of the ring and deshielding, often substantial, of the protons inside the ring. The paratropic ring current is thus a reversal of the more common diatropic current associated with aromaticity. It should be noted that the energetic and magnetic criteria of antiaromaticity do not always coincide (resonance destabilization versus paratropicity), as was pointed out by Aihara⁴⁸ and others.⁴⁹ However, in the following discussion, the antiaromaticity will be quantified chiefly on the basis of the experimentally observed paratropic ring current.

Porphyrins and their analogues are usually aromatic in the Hückel sense; that is, the macrocycle contains a closed circuit (delocalization pathway) containing $4n + 2 \pi$ electrons. The porphyrin itself contains an 18 π -electron pathway and can be labeled [18]porphyrin to emphasize the formal analogy with [18]-annulene.⁵⁰ Porphyrin derivatives containing $4n$ electron pathways, which could be expected to show antiaromatic behavior, are less common. They are normally obtained by two-electron reduction of [18]porphyrin (**1**) to [20]porphyrin (**11**, Scheme 5), often known as isophlorin. This approach was used by Müllen et al. to generate the antiaromatic dianion of zinc *meso*-tetra(*p*-tolyl)[20]porphyrin.¹⁴ The first neutral isophlorin was obtained by the group of Vogel via chemical reduction of a N,N',N'',N''' -tetramethylporphyrin dication.⁵¹ Related tetraoxa-

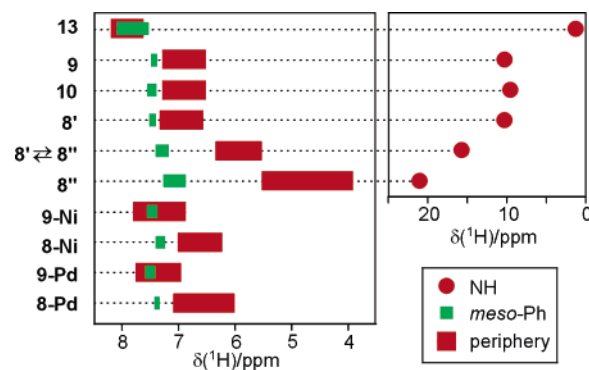


FIGURE 6. ^1H NMR chemical shift ranges for selected tetraphenylporphyrins and their metal complexes. Peripheral signals include those of the β -pyrrolic protons and the outer protons of the *meta*-phenylene (2,4-H and 3-H). For *para*-benzporphyrin **13**, the chemical shift of the outer *p*-phenylene signal (2,3-H) recorded at 183 K was included. For sources of previously published data, see references in the text.

and tetrathiaisophlorins were also made.^{50,52} Recently, a silicon complex of [20]porphyrin, $\text{Si}^{\text{IV}}(\text{TPP})(\text{THF})_2$, was reported by the group of Vaid.⁵³ This system was prepared by two-electron reduction of the respective tetraphenyl[18]porphyrin silicon complex $\text{Si}^{\text{IV}}(\text{TPP})\text{Cl}_2$ with sodium amalgam. The first systems containing a [16]porphyrin ring (**12**) were recently prepared by the group of Yamamoto by oxidation of dodecasubstituted [18]-porphyrins.⁵⁴ However, their macrocycles proved nonaromatic, probably due to significant out-of-plane distortion of the macrocycle caused by bulky peripheral substitution. Interestingly, a related lithium complex $[\text{Li}^{\text{I}}(\text{TPP})][\text{BF}_4]$, synthesized by Vaid and co-workers, also contains a 16 π -electron circuit but is planar enough to show significant paratropicity.⁵⁵

The above porphyrin-derived species usually have limited stability, as the porphyrin ring strongly favors its 18 π -electron aromatic state. Antiaromaticity is easier to attain in the case of expanded porphyrins,¹⁸ which can be attributed to the decreasing difference between resonance stabilization energies of $4n$ and $4n + 2$ systems for larger values of n .⁵⁶ Many of these systems have two accessible oxidation states, one of which exhibits macrocyclic aromaticity, whereas the other is antiaromatic.¹⁸ However, to date, paratropicity has never been observed in carbaporphyrinoids, even though some such systems contained appropriate $4n \pi$ -electron circuits.^{57,58}

In the present case, the phenolic tautomer $8'$ shows neither a diatropic nor a paratropic ring current and is nonaromatic as a macrocycle, similarly to other *m*-benzporphyrins.^{22,23} On the other hand, the paratropicity of the keto form $8''$ is evident from the unusual features of its ^1H NMR spectrum observed in the slow exchange limit. All of the signals of the peripheral protons of $8''$ are shifted upfield relative to their counterparts in $8'$. In

(40) Smirnov, S. N.; Golubev, N. S.; Denisov, G. S.; Benedict, H.; Schah-Mohammadi, P.; Limbach, H.-H. *J. Am. Chem. Soc.* **1996**, *118*, 4904.

(41) Golubev, N. S.; Shenderovich, I. G.; Smirnov, S. N.; Denisov, G. S.; Limbach, H.-H. *Chem.-Eur. J.* **1999**, *5*, 492.

(42) Shenderovich, I. G.; Burtsev, A. P.; Denisov, G. S.; Golubev, N. S.; Limbach, H.-H. *Magn. Reson. Chem.* **2001**, *39*, S91–S99.

(43) Tolstoy, P. M.; Schah-Mohammadi, P.; Smirnov, S. N.; Golubev, N. S.; Denisov, G. S.; Limbach, H.-H. *J. Am. Chem. Soc.* **2004**, *126*, 5621.

(44) Limbach, H.-H.; Pietrzak, M.; Sharif, S.; Tolstoy, P. M.; Shenderovich, I. G.; Smirnov, S. N.; Golubev, N. S.; Denisov, G. S. *Chem.-Eur. J.* **2004**, *10*, 5195.

(45) Sharif, S.; Denisov, G. S.; Toney, M. D.; Limbach, H.-H. *J. Am. Chem. Soc.* **2006**, *128*, 3375.

(46) Pople, J. A.; Untch, K. G. *J. Am. Chem. Soc.* **1966**, *88*, 4811.

(47) Lazzaretto, P. *Phys. Chem. Chem. Phys.* **2004**, *6*, 217.

(48) Aihara, J. *Bull. Chem. Soc. Jpn.* **2004**, *77*, 651.

(49) Cyrański, M. K.; Krygowski, T. M.; Katritzky, A. R.; Schleyer, P. v. R. *J. Org. Chem.* **2002**, *67*, 1333.

(50) Vogel, E. *Pure Appl. Chem.* **1993**, *65*, 143.

(51) Pohl, M.; Schmickler, H.; Lex, J.; Vogel, E. *Angew. Chem., Int. Ed. Engl.* **1991**, *30*, 1693.

(52) Vogel, E.; Pohl, M.; Herrmann, A.; Wiss, T.; König, C.; Lex, J.; Gross, M.; Gisselbrecht, J.-P. *Angew. Chem., Int. Ed. Engl.* **1996**, *35*, 1520.

(53) Cissel, J. A.; Vaid, T. P.; Rheingold, A. L. *J. Am. Chem. Soc.* **2005**, *127*, 12212.

(54) Yamamoto, Y.; Yamamoto, A.; Furuta, S.; Horie, M.; Kodama, M.; Sato, W.; Akiba, K.; Tsuzuki, S.; Uchamaru, T.; Hashizume, D.; Iwasaki, F. *J. Am. Chem. Soc.* **2005**, *127*, 14540.

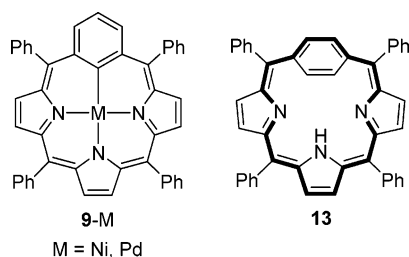
(55) Cissel, J. A.; Vaid, T. P.; Yap, G. P. A. *Org. Lett.* **2006**, *8*, 2401.

(56) Wiberg, K. B. *Chem. Rev.* **2001**, *101*, 1317.

(57) Hung, C.-H.; Wang, S.-L.; Ko, J.-L.; Peng, C.-H.; Hu, C.-H.; Lee, M.-T. *Org. Lett.* **2004**, *6*, 1393.

(58) Colby, D. A.; Ferrence, G. M.; Lash, T. D. *Angew. Chem., Int. Ed.* **2004**, *43*, 1346.

SCHEME 6

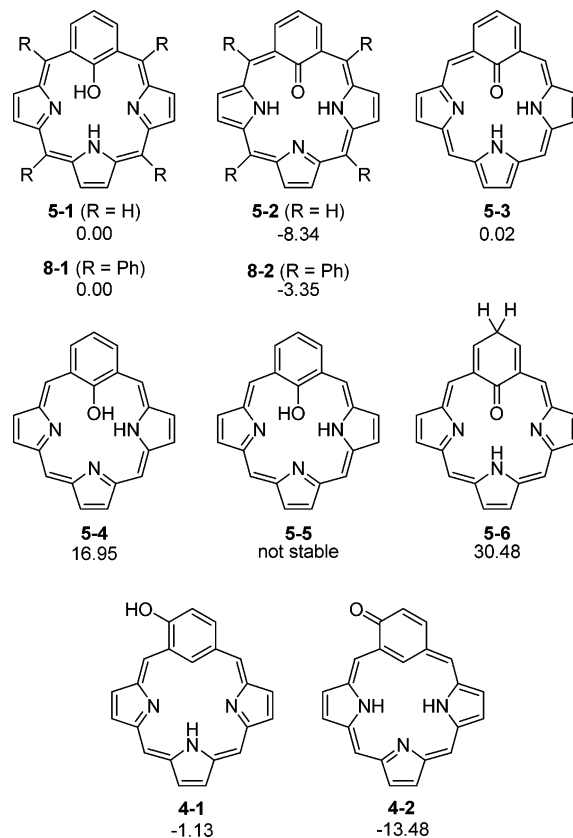


particular, the phenylene signal 2,4-H moves from 6.80 ppm, which is an acceptable value for an aromatic ring, to an unusually upfield position at 3.92 ppm. Paratropic shielding also affects the *meso*-phenyl rings, resulting in an upfield relocation of the ortho protons (to 6.88 ppm). On the other hand, the NH protons of **8''**, which are located inside the ring, are shifted to 21.0 ppm (at 193 K), more than 10 ppm downfield relative to the NH signal of **8'**.

Figure 6 shows a pictorial comparison of the ranges of proton chemical shifts observed for selected tetraphenylbenzporphyrins and their metal complexes. It is immediately noted that the chemical shift ranges for *m*-benzporphyrin **9**, and its 22-acetoxy- and 22-hydroxy derivatives (**10** and **8'**, respectively), are essentially identical. Tetraphenyl-*para*-benzporphyrin **13** shows strong diatropicity (Scheme 6),²⁴ which results in the expected deshielding of the outer protons and significant shielding of the inner NH. In sharp contrast to the above systems, 22-oxybenzporphyrin **8''** is paratropic, and the effect is also observable for the equilibrium mixture of **8'** and **8''** observed at 303 K. It is also apparent that the 22-hydroxybenzporphyrins of Ni(II) and Pd(II) (**8-Ni**, and **8-Pd**)²⁸ show residual paratropicity when compared to their *meta*-benzporphyrin counterparts (**9-Ni** and **9-Pd**).²³ The effect observed for **8-Ni** and **8-Pd** is weaker than in **8''**, which is likely due to the significant tilt of the phenolate in the complexes.²⁸

The antiaromaticity of **8''** can be explained in terms of a 20 π -electron circuit, which includes the peripheral part of the *m*-phenylene ring (Scheme 4). This circuit becomes directly available upon deprotonation of the phenolic OH group of **8**, which results in the formation of the semiquinone structure **8''**. Thus, the 22-hydroxy group acts as an antiaromaticity switch commuting the 6 π -electron benzenoid aromaticity of **8'** into the annulenoid antiaromaticity of **8''**. The function of the hydroxy group critically depends on its placement on the phenylene ring. In 2-hydroxy-*m*-benzporphyrin **4**, it provides access to an aromatic [18]annulenoid pathway present in **7**.²⁶ However, in that case, the keto tautomer **7** was formed exclusively, and no dynamic switching was observed.²⁶ On the other hand, the hydroxy group will be ineffective as a switch in 3-hydroxy-*m*-benzporphyrin (**6**), as no tautomers of **6** can be drawn that would exhibit macrocyclic aromaticity or antiaromaticity.

DFT Calculations. Density functional theory (DFT) has been successfully used to describe the properties of porphyrins and related systems, providing information on their energetics, conformational behavior, tautomerism, and aromaticity.⁵⁹ We have previously applied DFT modeling to study the relationship between aromaticity, tautomerism, and coordinating capabilities

SCHEME 7. Tautomers of 22-Hydroxy- and 2-Hydroxybenzporphyrin Used in the DFT Study^a

of 2-oxybenzporphyrin **7**.²⁷ In particular, we were able to reproduce the energetic preference of **7** to exist as the keto tautomer, and we showed that the corresponding phenolic structure could be stabilized upon metal coordination.

While the magnetic manifestations of aromaticity and antiaromaticity in the tautomers of **8** can easily be observed using ¹H NMR spectroscopy, this method does not provide detailed information on the energetic and structural consequences of electron delocalization in these two species. The coexistence of the two tautomers at comparable concentrations suggests that the energy difference between them is very small (of the order of kT), which is surprising because one of the systems is formally antiaromatic. Furthermore, in the absence of X-ray structural data, it is difficult to ascertain whether **8''** does exhibit bond alternation along the [20]annulene pathway, expected of a $4n$ π -electron system. Bond alternation in tetramethylisophlorin was observed in the solid state and in solution, and gave rise to valence tautomerism observable by ¹H NMR.⁵¹ In the present case, no clear indications of π -bond shifts were detected for **8''**, so the process is either absent or too fast to be detected in the available temperature range. To address these issues, we carried out DFT calculations of several tautomers of unsubstituted 22-hydroxybenzporphyrin **5** and its 2-hydroxy isomer **4** (Scheme 7), performing full geometry optimizations at the B3LYP/6-31G** level. In addition, phenyl-substituted variants of **5-1** and **5-2** (**8-1** and **8-2**) were also modeled. Structures **4-1** and **4-2** were reoptimized starting from previously published B3LYP/6-31G* models.²⁷

(59) Ghosh, A. Quantum Chemical Studies of Molecular Structures and Potential Energy Surfaces of Porphyrins and Hemes. In *The Porphyrin Handbook*; Kadish, K. M., Smith, K. M., Guillard, R., Eds.; Academic Press: San Diego, CA, 2000; Vol. 7, Chapter 47, pp 1–38.

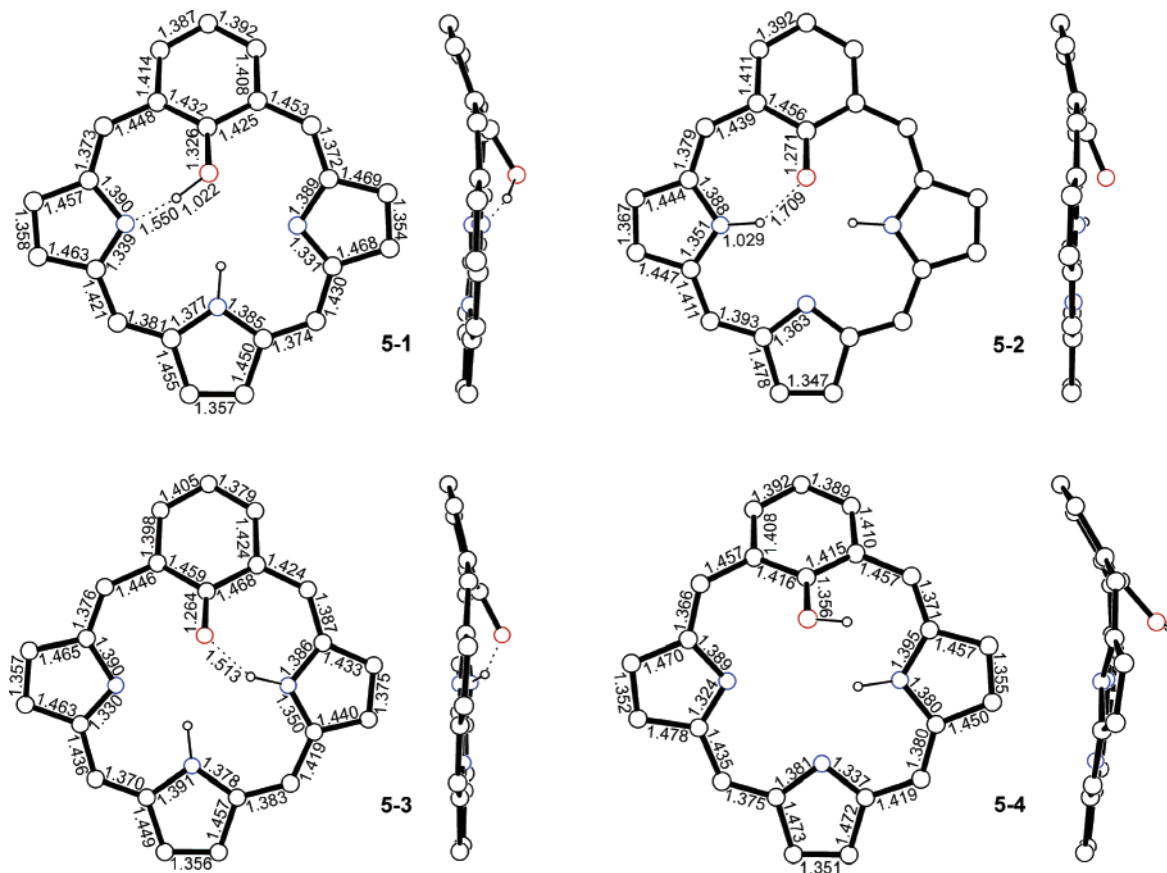


FIGURE 7. Calculated geometries and bond lengths of structures **5-1**–**5-4** optimized at the B3LYP/6-31G** level. Nitrogen and oxygen are shown in blue and red, respectively. Outer hydrogens are omitted for clarity. **5-2** has an effective C_s symmetry, and the equivalent bond distances are equal within the given accuracy.

Energy differences between the tautomers of **5** and **4** are given in Scheme 7 relative to **5-1**. Most importantly, the antiaromatic keto form **5-2** is found to be more stable than **5-1** by ca. 8 kcal/mol. In the pair of phenyl-substituted tautomers **8-1** and **8-2**, this energy gap decreases to ca. 3 kcal/mol. This result is still inconsistent with the experimental data, which show that the phenolic form **8'** (corresponding to **8-1**) dominates. However, the computational results correspond to isolated molecules, and the structure **8-1** will likely be stabilized in a polar solvent, such as dichloromethane.⁶⁰ A similar preference for a potentially destabilized keto tautomer was recently predicted by Hung et al. in an N-confused porphyrin derivative possessing a hydroxy group on the inner carbon.⁵⁷ Their DFT calculations indicated that the 20- π electron keto form is stabilized by 0.5 kcal/mol relative to the most stable enol form. Interestingly, this ordering was indeed reversed upon inclusion of a solvation model. Unfortunately, the compound could not be sufficiently characterized to provide support for these predictions.

The energies of the phenolic forms **5-1** and **4-1** are very similar, which is very suggestive but may result from an accidental compensation of several effects. For instance, **5-1** appears to be sterically more crowded than **4-1**, but it can benefit from intramolecular hydrogen bonding involving the OH group (vide infra). Interestingly, the energy difference between the two isomeric keto forms **5-2** and **4-2** is only 5 kcal/mol in favor of the latter. Structure **5-6**, included for reference, does not

contain any of the π -electron circuits available to other structures, and it is significantly destabilized.

The DFT-optimized geometries of structures **5-1**–**5-4** are shown in Figure 7. In each case, the tripyrrolic portion of the macrocycle is essentially planar, whereas the six-membered ring is slightly tilted out of the plane, so as to reduce steric congestion inside the macrocycle. The calculated geometry of **5-1** is conspicuous for a strong intramolecular hydrogen bond linking the phenolic OH group with one of the neighboring nitrogens. The $N\cdots H$ distance is only 1.550 Å, and the OH bond (1.022 Å) is elongated with respect to the calculated OH distance in phenol (0.966 Å, Supporting Information). More interestingly, the C(22)–O distance is 1.326 Å, which is shorter than the C–O bond length calculated for phenol (1.368 Å). In addition, the C_{ortho} – C_{ipso} distances in the phenol ring are longer than usual (1.432 and 1.425 Å for C(1)–C(22) and C(5)–C(22), respectively), indicating that the CO fragment has some double bond character. These structural features are consistent with the presence of a resonance-assisted hydrogen bond (RAHB)^{61–63} in **5-1**. The hydrogen bond closes a seven-membered ring, but the resonance involved in stabilization extends over the entire macrocycle. In the other stable phenolic conformer **5-4**, the OH group is turned away from the nitrogens and the hydrogen bond

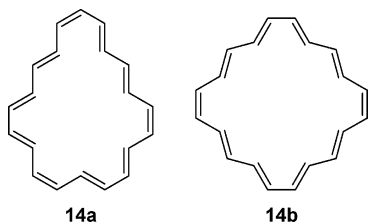
(61) Gilli, G.; Bellucci, F.; Ferretti, V.; Bertolasi, V. *J. Am. Chem. Soc.* **1989**, *111*, 1023.

(62) Sobczyk, L.; Grabowski, S. J.; Krygowski, T. M. *Chem. Rev.* **2005**, *105*, 3513.

(63) Bertolasi, V.; Gilli, G.; Ferretti, V.; Gilli, G. *J. Am. Chem. Soc.* **1991**, *113*, 4917.

(60) Ramos, M.; Alkorta, I.; Elguero, J.; Golubev, N. S.; Denisov, G. S.; Benedict, H.; Limbach, H.-H. *J. Phys. Chem. A* **1997**, *101*, 9791.

SCHEME 8. Two Configurations of [20]Annulene Corresponding to 20- π Electron Circuits Found in 5-2 and 11



is absent. In consequence, the CO distance becomes longer, and the system is significantly destabilized. The energy difference between **5-4** and **5-1** (17 kcal/mol) can largely be attributed to the absence of the O–H \cdots N bond in the former. We also tried to optimize structure **5-5**, which is similar to **5-4** except that the OH group is hydrogen bonded. However, our attempt to converge **5-5** resulted in an intramolecular proton transfer, and structure **5-2** was obtained instead. Thus, tautomer **5-5** does not correspond to an energy minimum at the employed level of theory.

It should be noted that the hydrogen-bonded structure **5-1**, while very interesting, is not unambiguously confirmed by the available low-temperature NMR data. The chemical shift of the OH group observed for **8'** at 193 K is 8.55 ppm, which is smaller than expected from a phenolic OH involved in intramolecular hydrogen bonding (usually above 10 ppm), but larger than the value recorded for phenol itself (5.35 ppm in CDCl₃).⁶⁴ Furthermore, in the slow exchange limit, the proton spectrum of **5-1** should exhibit lower symmetry. The effective C_s symmetry of **5-1** observed by NMR means that either the hydrogen bond switches rapidly between nitrogens 23 and 25 via libration of the OH group or no hydrogen bond is formed at all. In the actual molecule **8'**, the O–H \cdots N hydrogen bond may be weaker than suggested by the DFT model of **5-1**, as a consequence of *meso*-substitution, which can force the phenylene ring out of the macrocyclic plane. In fact, the hydrogen bond is slightly longer in the computed structure **8-1**, which includes *meso*-substituents, than in **5-1** (the N \cdots H distance of 1.676 versus 1.550 Å). Hydrogen bonding may be additionally weakened by interactions with the solvent.

Surprisingly, the optimized geometry of **5-2** shows no bond localization expected of an antiaromatic [4*n*]annulenoid system.^{51,53,55} While the bond distances along the [20]annulene circuit show some variability, no bond length alternation is observed, and the structure has a plane of symmetry intersecting the phenylene. This is in contrast with the known structures of 20 π -electron porphyrin rings: bond localization was experimentally observed in Vogel's tetramethylisophlorin⁵¹ and in Vaid's silicon isophlorin.⁵³ Arguably, this discrepancy could be caused by the difference in configurations of cis and trans bonds in the [20]annulenoid circuits in **5-2** and **11**. These configurations correspond to two different arrangements of the [20]annulene ring (**14a** and **14b**, respectively, Scheme 8). However, using the B3LYP/6-31G* level of theory, Schleyer et al. predicted bond alternation in **14a**,⁶⁵ which is incidentally the most stable configuration of [20]annulene.^{65,66} Furthermore,

using the same level of theory, Vaid et al. were able to correctly reproduce the experimental bond lengths in their antiaromatic porphyrin complexes,^{53,55} which also adds credibility to the B3LYP geometry of **5-2**.

To gain further computational insight into the structure of **5-2**, its geometry was additionally optimized using the Hartree–Fock (HF) approach and the new hybrid DFT method, known as KMLYP,⁶⁷ with the 6-31G** basis set (Table 1). While B3LYP is known to overestimate electron correlation, which may result in exaggerated bond equalization in aromatic systems, the HF formalism underestimates correlation contributions, often leading to spurious bond localization.⁶⁸ The KMLYP method, on the other hand, contains about 50% of the HF exchange contribution⁶⁷ and was recently shown by Schleyer et al. to yield correct geometries for several aromatic annulenes.⁶⁸ In the present case, the HF geometry of **5-2** indeed shows strong bond localization, whereas the KMLYP structure is symmetrical and quite similar to the B3LYP model. We can therefore conclude that the symmetrical structure of **5-2** is most probably correct. The absence of bond alternation in **5-2** is likely a result of a certain phenol-like contribution to the resonance structure of **5-2**, which may be assisted by intramolecular hydrogen bonding.

We attempted to analyze the above results in terms of the classical valence bond approach, which was hoped to provide an intuitive picture of the delocalization in **5-1** and **5-2**. Each structure can be thought of as a resonance hybrid of 12 canonical forms **a–l** depicted in Scheme 9, with the two protons placed appropriately for each tautomer (as in Scheme 7). The structures can be grouped into “phenolic” (**a–f**), each containing a formal single C–O bond, and “quinoidal” (**g–l**), containing C=O bonds. Within each set, the structures differ in the placement of formal negative charges on nitrogens and in the localization of double bonds on the [6]annulene or [20]annulene pathway (structures **a–f** and **g–l**, respectively). The degree of charge separation will depend on the protonation pattern of each tautomer. For instance, each of the tautomers **5-1** and **5-2** will only have two structures with no charge separation (**5-1a,d** and **5-2g,j**, respectively), and they can be accordingly expected to be the major contributors to the resonance. The weights of canonical structures **a–l** (Table 1 and Table S5, Supporting Information) were estimated from harmonic oscillator stabilization energies (HOSE) using the method proposed by Krygowski et al.^{69,70} In their approach, the weights are calculated from geometric information only (bond lengths) and can therefore also be used to analyze X-ray data.

HOSE resonance weights suggest that substantial mixing of phenolic and keto contributions occurs for all structures studied. This mixing is probably somewhat exaggerated; for instance, a keto contribution of ca. 30% is estimated for the ester derivative **10**. Surprisingly, the keto component, expressed as the sum of resonance weights of structures **g–l** (w_{g-l}), is only 10% higher for the 22-oxy tautomer **5-2** than for the 22-hydroxy tautomer **5-1**. This result is indicative of strong delocalization in both systems, which results in significant bond averaging. Interestingly, the highest w_{g-l} value (0.56) was obtained for the HF geometry of **5-2**, which features significant bond localization toward structure **g**.

(64) SDBSWeb. <http://www.aist.go.jp/RIODB/SDBS/> (National Institute of Advanced Industrial Science and Technology), 2006.

(65) Castro, C.; Isborn, C. M.; Karney, W. L.; Mauksch, M.; Schleyer, P. v. R. *Org. Lett.* **2002**, *4*, 3431.

(66) Metcalf, B. W.; Sondheimer, F. *J. Am. Chem. Soc.* **1971**, *93*, 6675.

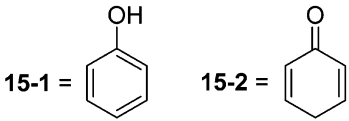
(67) Kang, J. K.; Musgrave, C. B. *J. Chem. Phys.* **2001**, *115*, 11040.

(68) Wannere, C. S.; Sattelmeyer, K. W.; Schaefer, H. F., III; Schleyer, P. v. R. *Angew. Chem., Int. Ed.* **2004**, *43*, 4200.

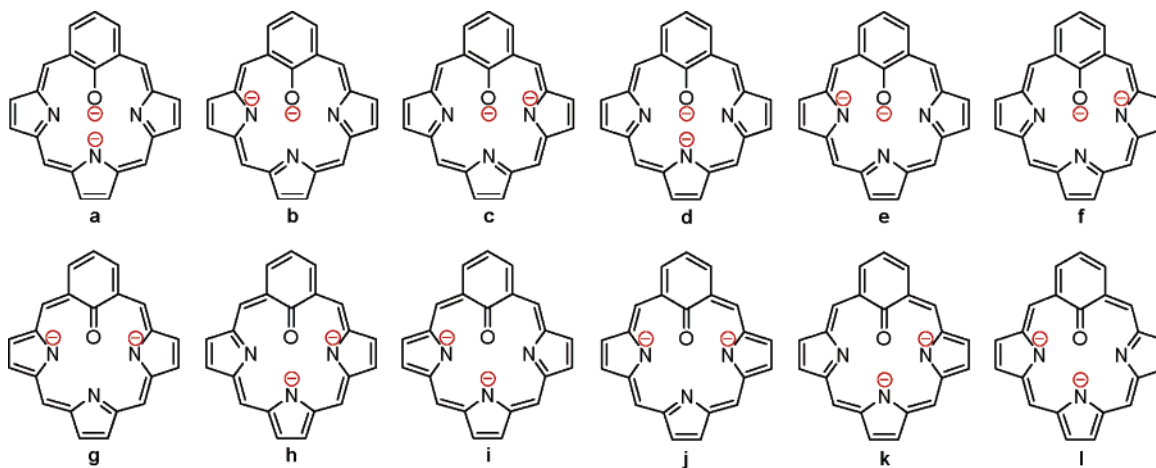
(69) Krygowski, T. M.; Anulewicz, R.; Kruszewski, J. *Acta Crystallogr., Sect. B* **1983**, *39*, 732.

(70) Krygowski, T. M.; Cyrański, M. K. *Chem. Rev.* **2001**, *101*, 1385.

TABLE 1. Delocalization Descriptors for 22-Hydroxybenzporphyrins and Reference Systems

System ^a	Wiberg bond indices ^{b,c}					HOSE resonance contributions ^{c,d}	
	C22–O	C1–C22	C5–C22	C1–C21	C5–C6	total keto (w_{g-1})	w_{\max}
5-1	1.08	1.29	1.29	1.12	1.10	0.36	0.13 (w_a, w_d)
5-2 (B3LYP)	1.34	1.17	1.17	1.17	1.17	0.46	0.09 (w_a, w_d)
5-2 (KMLYP)	1.33	1.17	1.17	1.16	1.16	0.45	0.10 (w_a, w_d)
5-2 (HF)	1.52	1.09	1.07	1.45	1.07	0.56	0.19 (w_g)
5-3	1.39	1.14	1.15	1.13	1.14	0.47	0.11 (w_d, w_k)
5-4	1.01	1.31	1.33	1.08	1.09	0.34	0.15 (w_c, w_f)
8-1						0.34	0.14 (w_a, w_d)
8-2						0.46	0.09 (w_a, w_d)
8-Pd^e						0.37	0.12 (w_a, w_d)
10^c						0.29	0.16 (w_a, w_d)
	C–O	C1–C2	C1–C6				
15-1	0.98	1.40	1.37				
15-2	1.70	1.04	1.04				

^a Unless noted, geometries come from B3LYP calculations. ^b Wiberg indices based on natural bond orbitals. Atom numbering for the benzporphyrin macrocycle follows that given in Scheme 1. ^c Full data are given in the Supporting Information. ^d w_{g-1} is the sum of all keto contributions (w_g through w_1); w_{\max} is the largest resonance weight for each system. ^e Published X-ray geometries.^{23,24}

SCHEME 9. Canonical Structures Used for the Estimation of Resonance Weights^a

^a For each tautomer, the placement of inner protons is given in Scheme 7.

As an alternative to the cumulative picture provided by resonance weights, we decided to estimate orders of pertinent bonds in the tautomers of **5**, using Wiberg bond indices (Table 1). In particular, C–O bond orders calculated for **5-1** and **5-2** are 1.08 and 1.34, respectively, which again shows that there is a significant phenolic component in **5-2**, and a slight keto admixture in **5-1**. For comparison, in the two tautomers of phenol **15-1** and **15-2** (Table 1), the C–O bond orders are 0.98 and 1.70, respectively, setting the feasible limits for “pure” phenolic and keto structures.

NICS Calculations. Nucleus-independent chemical shifts (NICS) have been proposed by Schleyer et al. as a computational measure of aromaticity that is related to experimental magnetic criteria.^{71,72} A NICS is defined as the negative shielding value computed at the geometric center of a ring. For monocyclic systems, NICS values generally correlate well with other

(71) Schleyer, P. v. R.; Meaerker, C.; Dransfeld, A.; Jiao, H.; Hommes, N. J. R. v. E. *J. Am. Chem. Soc.* **1996**, *118*, 6317.

(72) Chen, Z.; Wannere, C. S.; Corminboeuf, C.; Puchta, R.; Schleyer, P. v. R. *Chem. Rev.* **2005**, *105*, 3842.

established aromaticity criteria^{71,72} (the validity of these correlations was, however, disputed^{73–75}), but they are less conclusive for polycyclic molecules. Nevertheless, the NICS method has been used to assess the aromaticity of porphyrins^{76,77} and their analogues.⁷⁸ It has been argued that NICS values should only be used as descriptors of local aromaticity (and, in fact, each NICS is only locally defined) and not to quantify the aromaticity of the entire molecule.⁷⁹ Bearing this restriction in mind, we decided to perform a NICS analysis for selected benziporphyrins and compare the results with the experimental data.

NICS values were calculated for molecules **2**, **3**, **5-1**, **5-2**, **4-1**, and **4-2** at the centers of the phenylene ring and the three pyrrole rings. In addition, the NICS value for the central 16-membered ring (center ring) was obtained in each case (oxygen atoms were ignored in the calculation of ring centers). The results are depicted in Figure 8, with red and green circles representing, respectively, aromaticity and antiaromaticity (exact values are given in the Supporting Information). Comparison of the center ring NICS values shows that they are good indicators of macrocyclic aromaticity. For the aromatic systems **3** and **4-2**, the central NICS values are negative and comparable to that reported for porphyrin (**1**).⁷⁶ On the other hand, for the nonaromatic forms **2**, **5-1**, and **4-1**, these NICS values are small in magnitude (−0.2 to +0.8), indicating that the macrocyclic aromaticity is not well defined. Finally, for the antiaromatic 22-oxybenzporphyrin **5-2**, the center ring NICS is +5.0, which is the largest positive value among the investigated macrocycles. It is smaller than the NICS obtained for [20]annulene **14a** (+12.1),⁶⁵ but due to structural differences between **5-2** and **14a** these values cannot be directly compared.

The values obtained for pyrrole rings can be interpreted as resulting from the superposition of the local aromaticity of pyrrole and the macrocyclic aromaticity of the entire molecule. For the nonaromatic molecules **2**, **5-1**, and **4-1**, the pyrrole NICS values are invariably smaller, in the absolute sense, than the reference NICS calculated for the parent pyrrole ring (−15.1),⁷¹ suggesting that the local aromaticity is attenuated in the conjugated tripyrrolic unit. On the other hand, in the aromatic macrocycles **3** and **4-2**, the pyrrole NICS values are differentiated similarly as in porphyrin **1**.⁷⁶ Those pyrrole ring centers that reside inside the formal [18]annulene path yield larger negative values than the ring centers outside this path. No reversal of this trend is seen for the antiaromatic **5-2**, but the NICS values of pyrrole rings indicate a decrease in their local aromaticity. In the nonaromatic benziporphyrins **2**, **5-1**, and **4-1**, the phenylene NICS is in each case similar to the reported benzene NICS.⁷¹ The phenylene NICS takes a larger absolute value in *p*-benzporphyrin **3**, where it is probably affected by macrocyclic aromaticity. Interestingly, the phenylene NICS is positive and fairly large in **5-2** and **4-2**, the two structures with a semiquinone benzene ring. Even though similar results were obtained for quinones,⁷² this similarity may be only accidental.

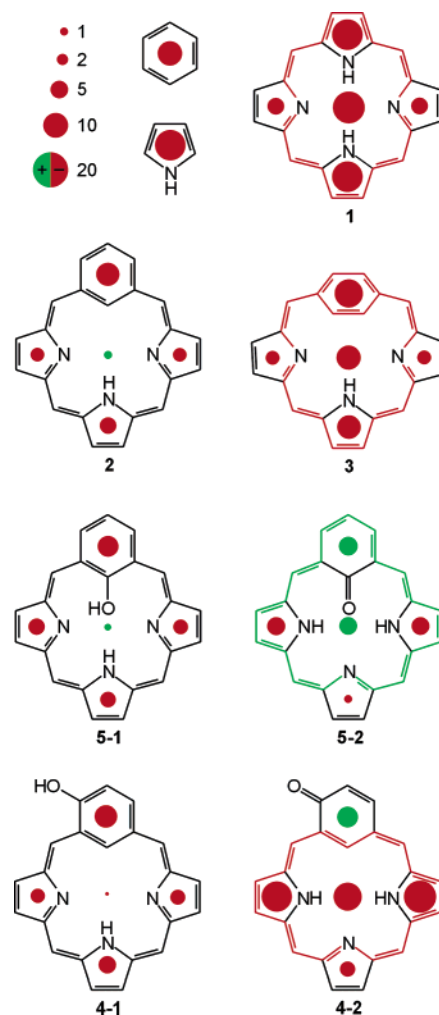


FIGURE 8. Nucleus-independent chemical shifts (NICS, GIAO-RHF/6-31G**) calculated for selected benziporphyrins. Negative (“aromatic”) NICS values are shown as red circles with the area proportional to the value. Positive NICS values are in green. For comparison, data for pyrrole,⁷¹ benzene,⁷¹ and porphyrin (**1**)⁷⁶ are included.

Conclusions

The present work provides an unprecedented example of a tautomerization process that acts as a switch of antiaromaticity. The two tautomers of 22-hydroxybenzporphyrin, the phenolic species **8'** and its companion keto form **8''**, have very similar energies and coexist in solution over a wide range of temperatures. The very fast tautomerization process can be slowed down with the help of low temperatures and deuterium isotope effect, making it possible to directly observe **8'** and **8''** using ¹H NMR spectroscopy. Computational results suggest that the possibility to simultaneously observe the two species may result from fortuitous cancellation of several energetic contributions, involving aromaticity, antiaromaticity, hydrogen bonding, and steric effects. This cancellation was not achieved in the isomeric 2-hydroxybenzporphyrin system, for which only the aromatic keto form was previously observed. Our results indicate that, in appropriately designed systems, electron delocalization and aromaticity can be dynamically controlled by inclusion of tautomerizing functionalities. Further work exploring the generality of this approach is in progress in our laboratory.

(73) Katritzky, A. R.; Barczynski, P.; Musumarra, G.; Pisano, D.; Szafran, M. *J. Am. Chem. Soc.* **1989**, *111*, 7.

(74) Katritzky, A. R.; Karelson, M.; Sild, S.; Krygowski, T. M.; Jug, K. *J. Org. Chem.* **1998**, *63*, 5228.

(75) Jug, K.; Köster, A. M. *J. Phys. Org. Chem.* **1991**, *4*, 163.

(76) Cyrański, M. K.; Krygowski, T. M.; Wisiorowski, M.; Hommes, N. J. R. v. E.; Schleyer, P. v. R. *Angew. Chem., Int. Ed.* **1998**, *37*, 177.

(77) Jusélius, J.; Sundholm, D. *J. Org. Chem.* **2000**, *65*, 5233.

(78) Furuta, H.; Maeda, H.; Osuka, A. *J. Org. Chem.* **2001**, *66*, 8563.

(79) Krygowski, T. M.; Cyrański, M. K.; Czarnocki, Z.; Häfelfinger, G.; Katritzky, A. R. *Tetrahedron* **2000**, *56*, 1783.

Experimental Section

Materials. The dichloride salt of 6,11,16,21-tetraphenyl-22-hydroxy-*m*-benzporphyrin **8**·2HCl was obtained as described previously.²⁸ Deuterated solvents were used as received, except for chloroform-*d*, which was deacidified by passing down a basic alumina column.

6,11,16,21-Tetraphenyl-22-hydroxy-*m*-benzporphyrin (8**).** In the following procedure, an inert atmosphere was maintained at all times: **8**·2HCl (14.3 mg, 0.02 mmol) was placed in a 25 mL flask equipped with a septum cap and a stir bar and was dissolved in oxygen-free CH₂Cl₂ (5 mL). Aqueous NaOH was added (1 M, 5 mL), and the resulting mixture was stirred for 5 min at room temperature. The phases were then allowed to separate, and the organic phase was withdrawn with a syringe, transferred to a flask containing water (10 mL), and stirred for 5 min. The organic phase was again separated and transferred to a new flask, and the solvent was removed under reduced pressure. The resulting sample of **8** was subsequently dried under high vacuum for several hours and transferred to a glove box. NMR samples of **8** were prepared immediately. The deuterated derivative **8**-*d*₂ was prepared in a similar manner, NaOH and water being replaced by their deuterated analogues.

NMR Spectroscopy. ¹H NMR spectra were recorded on a high-field spectrometer (¹H frequency 500.13 MHz), equipped with a broadband inverse gradient probehead. Spectra were referenced to the residual solvent signals (chloroform-*d* 7.24 ppm, dichloromethane-*d*₂ 5.32 ppm, toluene-*d*₈ 2.09 ppm). Two-dimensional NMR spectra were recorded with 2048 data points in the *t*₂ domain and up to 1024 points in the *t*₁ domain, with a 0.5–1 s recovery delay. The TOCSY spectrum shown in Figure 2 was recorded using a MLEV-17 spinlock of 40 ms duration. The EXSY spectrum (Figure 3) was obtained using a conventional NOESY sequence with a mixing time of 400 ms. Rate constants were calculated from linewidths of selected signals using typical approximations for the fast and slow exchange. In the slow exchange limit, the rate *k* is given as:

$$k = \pi\nu_{1/2}$$

where $\nu_{1/2}$ is the line width. In the fast exchange limit, the equations for an unequally populated system were used:

$$k_{A \rightarrow B} = 4\pi p_A p_B \frac{\Delta\nu^2}{\nu_{1/2}}$$

where p_A and p_B are populations of the exchanging species, and $\Delta\nu$ is the difference of chemical shifts (in Hz) between the signals under slow exchange. $\Delta\nu$ values were obtained from the spectrum of **8**-*d*₂ at 193 K. Populations p_A and p_B were estimated from the positions of coalesced signals in the fast exchange limit. The linewidths $\nu_{1/2}$ were corrected for inhomogeneous broadening by

subtraction of a reference line width. Scalar coupling was assumed to have a negligible effect on the validity of the equations used. However, the linewidths of multiplets were corrected by subtraction of the corresponding coupling constants.

Computational Chemistry. Density functional theory calculations were performed using Gaussian 03.⁸⁰ Geometry optimizations were carried out within unconstrained C₁ symmetry, with starting coordinates preoptimized using semiempirical methods. Becke's three-parameter exchange functional⁸¹ with the gradient-corrected correlation formula of Lee, Yang, and Parr (B3LYP)⁸² was used with the 6-31G** basis set. The KMLYP method was implemented as described in the literature.⁶⁷ With the exception of **8**-**1** and **8**-**2**, harmonic vibrational frequencies were calculated for all systems using analytical second derivatives. The structures were found to have converged to a minimum on the potential energy surface; the resulting zero-point vibrational energies were included in the calculation of relative energies (Scheme 7). NICS values were calculated at the GIAO-RHF/6-31G** level of theory using the B3LYP geometries.

Acknowledgment. Financial support from the Ministry of Science and Higher Education (grant PBZ-KBN-118/T09/2004) is kindly acknowledged. Quantum chemical calculations have been carried out at the Poznań Supercomputer Center (Poznań) and Wrocław Supercomputer Center (Wrocław). We wish to thank one of the reviewers for a helpful discussion of the tautomeric equilibria.

Supporting Information Available: Tables of computational results (Cartesian coordinates, tables) and additional NMR data. This material is available free of charge via the Internet at <http://pubs.acs.org>.

JO0623437

(80) Frisch, M. J.; Trucks, G. W.; Schlegel, H. B.; Scuseria, G. E.; Robb, M. A.; Cheeseman, J. R.; Montgomery, J. A., Jr.; Vreven, T.; Kudin, K. N.; Burant, J. C.; Millam, J. M.; Iyengar, S. S.; Tomasi, J.; Barone, V.; Mennucci, B.; Cossi, M.; Scalmani, G.; Rega, N.; Petersson, G. A.; Nakatsuji, H.; Hada, M.; Ehara, M.; Toyota, K.; Fukuda, R.; Hasegawa, J.; Ishida, M.; Nakajima, T.; Honda, Y.; Kitao, O.; Nakai, H.; Klene, M.; Li, X.; Knox, J. E.; Hratchian, H. P.; Cross, J. B.; Bakken, V.; Adamo, C.; Jaramillo, J.; Gomperts, R.; Stratmann, R. E.; Yazyev, O.; Austin, A. J.; Cammi, R.; Pomelli, C.; Ochterski, J. W.; Ayala, P. Y.; Morokuma, K.; Voth, G. A.; Salvador, P.; Dannenberg, J. J.; Zakrzewski, V. G.; Dapprich, S.; Daniels, A. D.; Strain, M. C.; Farkas, O.; Malick, D. K.; Rabuck, A. D.; Raghavachari, K.; Foresman, J. B.; Ortiz, J. V.; Cui, Q.; Baboul, A. G.; Clifford, S.; Cioslowski, J.; Stefanov, B. B.; Liu, G.; Liashenko, A.; Piskorz, P.; Komaromi, I.; Martin, R. L.; Fox, D. J.; Keith, T.; Al-Laham, M. A.; Peng, C. Y.; Nanayakkara, A.; Challacombe, M.; Gill, P. M. W.; Johnson, B.; Chen, W.; Wong, M. W.; Gonzales, C.; Pople, J. A. *Gaussian 03*, revision C.02; Gaussian, Inc.: Wallingford, CT, 2004.

(81) Becke, A. D. *Phys. Rev. A* **1988**, *38*, 3098.

(82) Lee, C.; Yang, W.; Parr, R. G. *Phys. Rev. B* **1988**, *37*, 785.